Published in final edited form as:
Nat Methods. 2015 September ; 12(9): 831–834. doi:10.1038/nmeth.3506.

EEG and functional ultrasound imaging in mobile rats

Lim-Anna Sieu[1,3], **Antoine Bergel**[1,4], **Elodie Tiran**[2], **Thomas Deffieux**[2], **Mathieu Pernot**[2], **Jean-Luc Gennisson**[2], **Mickaël Tanter**[2], and **Ivan Cohen**[1]

[1]INSERM U1130, CNRS UMR8246, University Pierre & Marie Curie UMCR18, Paris, France

[2]Institut Langevin, ESPCI ParisTech, PSL Research university, CNRS UMR7587, INSERM U979, Paris, France

[3]Institut de recherche translationnelle en Neurosciences ICM-A-IHU, Paris, France

[4]Université Paris Diderot, Sorbonne Paris Cité, Ecole Doctorale Frontières du Vivant (FdV), Programme Bettencourt, Paris, France

Abstract

We developed an integrated experimental framework which extends the brain exploration capabilities of functional ultrasound imaging to awake/mobile animals. In addition to hemodynamic data, this method further allows parallel access to EEG recordings of neuronal activity. This approach is illustrated with two proofs of concept: first, a behavioral study, concerning theta rhythm activation in a maze running task and, second, a disease-related study concerning spontaneous epileptic seizures.

In vivo brain activity recordings provide a unique contribution to neuroscience to unravel the underlying mechanisms of complex behaviors and pathologies. Ideally we would like to capture instantly both neuronal activity and metabolic events, which form two major facets of global brain equilibrium, in the most natural conditions, that is when the subject is awake and freely moving. There is an increasing awareness today that major issues of neurophysiology need to be addressed with such global approaches. Notably, the basic mechanisms involved in functional network dynamics and pathologies including epilepsy can be deciphered only if the electrographic and metabolic components are sensed concomitantly [Logothetis 2008, Sada 2015]. More generally, the multiple feedbacks between electrographic and metabolic signals represent the rule, rather than the exception. They have been tackled separately only by lack of appropriate methods for accessing the global picture, prompting the development of multimodal strategies.

In practice there is a compromise between the size of imaging field, time resolution, sensitivity, separability of processing and metabolism, and physical constraint on the animal.

Corresponding author: IC, ivan.cohen@upmc.fr.

Author contributions

LAS designed the surgical procedure and prosthetic skull, and performed and analyzed epilepsy experiments; AB designed intra-hippocampal recording procedure and performed and analyzed navigation experiments; ET and TD developed the “burst mode” ultrasound recording sequence; MP and JLG developed the “continuous mode” ultrasound recording sequence; JLG and MT designed and supervised the ultrasound scanner and probe; IC designed and supervised the experiments, designed the probe holder, programmed acquisition and analysis software; IC, LAS, AB wrote the paper.

Europe PMC Funders Author Manuscripts

Electrophysiology and more recently optical techniques [Kerr 2012, Packer 2015] can record neuronal activity in the mobile animal, yet sampling is limited, respectively, by electrode size and light diffraction. Conversely, fMRI records brain-wide metabolic adaptation, with tradeoffs in sensitivity and resolution, at the cost of subject immobilization or animal sedation [Logothetis 2008]. Recently introduced functional ultrasound imaging based on ultrafast Doppler (fUltrasound) offers a way to monitor brain hemodynamics [Macé 2011, Macé 2013] and functional connectivity [Osmanski 2014] in rodents with high spatiotemporal resolution and unique sensitivity. However, the screening nature of the skull to ultrasound waves required the removal of the bone and application of the ultrasound probe directly above the tissue, bathed in ultrasound conductive saline, in an immobile, anesthetized animal.

To unfold the potential of fUltrasound we develop here the proof of concept for the extension of the technique to awake and mobile rats (mfUS). Furthermore, in such condition we demonstrate the possibility to combine recording of cerebral hemodynamics at high spatiotemporal resolution and sensitivity, with simultaneous monitoring of neuronal activity through EEG. We have developed an integrated experimental setup that relies on a set of technological advances: an ultrasound permeable skull prosthesis, a lightweight ultrasound probe, a motorized head-mounted probe holder, electrode implantation procedure and software environment for synchronized acquisition, playback and analysis of these multimodal signals.

We present the details of this general experimental framework below (Fig. 1) and then we demonstrate two tailored applications (Fig. 2), first to search for the functional correlate of theta rhythm, known to be involved in brain area communication in spatial navigation tasks [Buzsaki 2013], and, second, to explore the neuronal and metabolic manifestations of spontaneous generalized epileptic seizures, as how absence seizures initiate and generalize remain a debated question with clinical impact [David 2008, Zheng 2012, Jacobs 2009].

In mfUS we first prepare the animal with a new surgical procedure (Supplementary Fig. 1, Supplementary Fig. 2), then we later proceed with the chronic recording sessions (Fig. 1a). Craniotomy of the parietal and frontal skull bones (15 mm AP × 14 mm ML) exposes the dura mater. Intracranial stereotaxic electrodes, either hippocampal (Supplementary Fig. 3), or cortical, are implanted, anchored on the edges of the window and their connector is fixed to the back of the head. Finally, a polymer prosthesis is sealed in place of the skull. The material that offers the best images is polymethylpentene film of 125μm thickness, further providing good mechanical resistance and low permeability. Thus we achieve observational access to the cortex and deep structures, with larger and deeper field of view, and improved sensitivity over earlier cranial thinning procedures [Osmanski 2014]. Three nuts used as attachment points for the probe holder are sealed above the nasal and lateral to the interparietal bones, and the animal is allowed a recovery period. Ultrasound recordings use a miniature ultrasound probe (18 mm radius, 25 mm height) mounted on a lightweight head-anchored adjustable holder (18 g, Supplementary Fig. 4, Supplementary Fig. 5). The device is fixed to the head under short isoflurane anesthesia, with contact gel between the probe and prosthetic skull. The holder is motorized (Supplementary Fig. 6) to explore consecutive

planes, without direct interaction between the experimenter and the animal, and can be locked for maximum stability.

We first recorded from rats walking along a linear maze, to address how brain-wide networks activate during periods of hippocampal theta rhythm, which is a major mechanism proposed for intracerebral cross-area processing in episodic memory and spatial navigation tasks [Buzsaki 2013]. Healthy Sprague Dawley rats (n=8) ran on a 2.25 m long, 0.2 m wide linear track for water reward. A single imaging plane included dorsal hippocampus, cortex with somatosensory areas, and thalamus. In order to temporally resolve hemodynamics as the animal crossed the maze we used a "burst mode" ultrasound sequence (Fig. 1b, Supplementary Fig. 7), acquiring fUS compound frames at 500 Hz for 12 s. Acquisition was triggered when the animal turned around, and was followed by a 40 s lapse to collect the data. Hippocampal electrodes were used. As expected, hippocampal theta was consistently associated with locomotion. Distance travelled over time was shorter (56-64%) than in control untethered, surgery-free, rats ($p<10^{-6}$, Supplementary Fig. 8a, b, tables 1 and 2). Yet, maximum speed was only slightly slower for the initial 15min, with the difference reducing to non significant 1% thereafter. In order to analyze series of track crossing trials, we aligned them by setting each trial reference time when the rat crossed the middle of the maze.

In this experiment single pixel variations, relative to average baseline when the animal is at rest, ranged from −30% to +60% (Fig. 1b), while brain area averages reached −10% to +20% (Fig. 2b). As expected, theta band intra-hippocampal EEG power peaked at top animal speed, which was coincident with crossing the midline, with a mid-height theta peak width of 3.2+/−0.3 s (n=8). In order to quantify functional activation during the task, we computed the maps of Pearson's correlation coefficient between power in the theta band and pixel intensity, for varying time lags (Fig. 2a). Averaging pixels across anatomical areas revealed hyper-perfusion in the somatosensory cortex, dorsal thalamus and hippocampus, and hypo-perfusion in the ventral thalamus. These correlations were consistent with fUltrasound signal time course (Fig. 2b). Hyperemia peaked at 0.7-1.5 s following the peak of hippocampal theta, which is compatible with signaling cascades that adapt blood flow to cognitive demand implied by the task [Koehler 2009]. The occasional asymmetry that we observed between left and right cortical hemispheres may correlate with functional dominance [LaMendola 1997]. Overall (Fig. 2c), our data reveal a pattern of combined hippocampal and widespread cortical activation in a short time window around the navigation task, with coordinated thalamic suppression. This pattern is coherent with observations in still animals, in the context of spontaneous activity during a conditioning protocol [Logothetis 2012], which described thalamic suppression during hippocampo-cortical interaction involved in episodic memory operations. In the present locomotion task, the dorsal thalamus is activated simultaneously with a suppression in the ventral thalamus.

In a second experiment we scanned through the brain of an epileptic rat, to address the heterogeneous alterations in neuro-metabolic coupling during hypersynchronous seizure activity [Sada 2015]. Spontaneous generalized absence seizures were recorded from bilateral cortical bipolar electrodes in Genetic Absence Epilepsy Rats from Strasbourg (GAERS, n=12). We quantified both the relative time spent seizing and seizure duration, and found no

significant difference between EEG only and EEG-mfUS conditions (Supplementary Fig. 8c, d, table 3). A “continuous mode” of ultrasound acquisition was used (Fig. 1c, Supplementary Fig. 7), alternating 200ms to generate one compound mfUS image followed with 2.8 s of processing. Multiple imaging planes were scanned for 10-15min each.

In this experiment, we also found individual pixel changes in the range from −30% to +60%, relative to seizure-free baseline, (Fig. 1c), while averaging over seizure-associated areas revealed changes from −10% to +20% (Fig. 2e, f). We found distinct patterns of correlation across structures along the antero-posterior axis. Hyper-perfusion in the somatosensory cortex and thalamus was concomitant with hypo-perfusion in the Caudate Putamen (CPu) and no variation in the hippocampus. Although absence seizures are generalized throughout neocortex, vascular alterations showed spatial compartments, and lateralization in the frontal primary sensory cortex perfusion was observed in half of the animals [6/12 rats]. Furthermore, the sensitivity of mfUS revealed that consecutive seizures with a similar bilateral cortical EEG profile could display distinct bilateral or unilateral perfusion course (Fig. 2e). Comparing the dynamics of cortical and thalamic areas coupled to seizure (Fig. 2f) revealed synchronous oscillations in the perfusion pattern. Thus, the responses we observed across anatomical structures (Fig. 2g) are compatible with EEG-fMRI experiments that found inversed electrographic-hemodynamic coupling between the cortex and CPu [Mishra 2011], and with time-resolved EEG-NIRS experiments that indicate blood flow fluctuations around seizures initiation [Roche-Labarbe 2010]. With the best of time and spatial resolution of these two techniques, mfUS further points to cortical decoupling between electrographic activity and perfusion, with both static and transient components, in naturally occurring seizures.

We have developed a new experimental tool that captures the hemodynamic state of the brain over its whole depth along with its electrographic activity in awake, mobile rats over repeated and prolonged periods of time. Despite the small size and weight of the probe, holder and cable, the system limits the distance and environment that the animal can explore, in a way similar to multichannel microdrive tetrode recordings. Another limitation is a potential contribution of a locomotion effect to brain perfusion, for instance due to higher heart rate during running. Absence seizures correspond to animal freezing and still showed strong variations in hemodynamics. Furthermore, such a locomotion effect is expected to be uniform across brain areas, while we found both increases and decreases in perfusion, even in the running task. Thus we exclude a locomotion effect in the tasks presented here, although it may become apparent during more intensive locomotion activity.

In two illustrative paradigms we demonstrated how this tool applies to both cognitive and pathological questions. Thus, significant progress was achieved to observe the interplay between metabolism and neuronal electrical activity that govern global brain equilibrium. While current plane-by-plane imaging could be adapted to address questions such as hippocampal-prefrontal cortex interaction [O'Neill 2013, Brincat 2015] by rotating the probe from the current coronal orientation, synchronous volumic acquisition will become possible with future matrix-type probes. As it develops, functional ultrasound imaging becomes applicable to a wide range of protocols including complex behavioral tasks in healthy animals and neurovascular pathologies.

Europe PMC Funders Author Manuscripts

Online Methods

Animal preparation

All animals received humane care in compliance with the European Communities Council Directive of 2010 (2010/63/EU), and the study was approved by the institutional and regional committees for animal care. Adult Sprague Dawley rats aged 10-12 weeks and GAERS (Genetic Absence Epilepsy Rat from Strasbourg) aged 8-16 weeks underwent surgical craniotomy and implant of ultrasound-clear prosthesis. Anesthesia was induced with 2% isoflurane and maintained by ketamine/xylazine (80/10 mg/kg), while body temperature was maintained at 36.5°C with a heating blanket (Bioseb, France). A sagittal skin incision was performed across the posterior part of the head to expose the skull. Parietal and frontal flaps were excised by drilling and gently moving the bone away from the dura mater. The opening exposed the brain between the olfactory bulb and the cerebellum, from Bregma +6 to Bregma −8mm, with a maximal width of 14mm. Electrodes were implanted stereotaxically and anchored on the edge of the flap. A plastic sheet of polymethylpentene was sealed in place with acrylic resin (GC Unifast TRAD) and residual space was filled with saline. We chose a prosthesis approach which offers larger field of view and prolonged imaging condition over 1-2 month, compared to the thinned bone approach [Osmanski 2014]. Particular care was taken not to tear the dura in order to prevent cerebral damage. The surgical procedure, including electrode implantation, typically took 4-6h. Animals recovered quickly, and after a conservative one week resting period they were used for data acquisition.

In order to attach the ultrasound probe and connect the EEG before a recording session, rats undergo short anesthesia for 20-25 min with 2% isoflurane. Acoustic gel is applied on the skull prosthesis, then the probe is inserted into the holder. The gel does not dry out even for extended recordings of up to 6-8 h. Animals are allowed to recover for 30 min before starting the recording session.

Electrodes

Electrodes are based on regular polytrodes made of bundles of insulated tungsten wires, either multisite (for hippocampal theta) or bipolar (for epilepsy). The difference with standard design is the right angle elbow that is formed prior to insertion in the brain (Supplementary Fig. 2). This shape allows to anchor the electrodes on the skull anterior or posterior to the flap. Electrodes are implanted with stereotaxic positioning micromotion and anchored one after the other, then the plastic film is applied to seal the skull. Two epidural screws placed above the cerebellum are used as reference and ground.

Intra-hippocampal handmade theta electrode bundles are composed of 25 μm insulated tungsten wire, soldered to miniature connectors (Supplementary Fig. 3). Four to six conductive ends are spaced by 1mm and glued to form 3 mm-long, 50 μm thick bundles. The bundles are lowered in dorsal hippocampi at stereotaxic coordinates AP = −4, ML = +/− 2.5, DV = −1.5 to −4.5, in mm relative to Bregma. Hippocampal theta rhythm is confirmed by phase inversion across recording sites in successive hippocampal layers, time-frequency decomposition, and coincidence with periods of exploration and navigation.

Europe PMC Funders Author Manuscripts

Cortical electrodes for absence epilepsy recordings used four bipolar electrodes implanted in primary somatosensory cortex: S1BF = AP −3, L +/− 5, DV −1,75 and S1Lp = AP +1, L +/− 6, DV −2, in mm relative to Bregma.

Skull prosthesis

The prosthetic skull is composed of polymethylpentene (PMP, Goodfellow, Huntington UK, goodfellow.com), a standard biopolymer used for implants. This material has tissue-like acoustic impedance, which allows undistorted propagation of ultrasound waves at the acoustic gel-prosthesis and prosthesis-saline interfaces. The prosthesis is cut out of a film of 125 μm thickness and sealed to the skull with resin.

Animal behavior

Animals for the maze experiment were trained before surgery. They were placed under a controlled water restriction protocol (weight between 85 and 90% of the normal weight) and trained to run back and forth in a long rectangular maze for water reinforcement. The maze (225 × 20 cm) had 5 cm high lateral walls, and was placed 50 cm above ground. Drops of water were delivered through two small tubes coming out from the two end walls of the maze (Fig. 1b). Each time the animal crossed the maze, a single drop of water was delivered in alternate water tubes by opening an electronically controlled pair of solenoid valves. Daily training lasted 30 min. Rats took about 2 sessions to reach a 60 crossing criterion and perform reliably, crossing the maze at fast speed, but were reinforced for at least two more days. Daily recording sessions lasted 20 to 30 min, depending on animal motivation. Since the acquisition in “burst mode” required 40 s for image reconstruction from ultrasound echoes, we could not capture every run. The number of runs acquired ranged from one fourth to one half of all the runs, depending on animal performance and the timing of its spontaneous runs within the session. The data analyzed here were recorded in 12 sessions performed across 8 days. Epileptic animals were recorded in a regular housing cage with cover removed.

Miniature ultrasound probe

The Ultrasonic probe (Vermon, Tours, France) is a linear array made of 128 transducers working at a 15MHz central frequency (spatial pitch 0.11mm, transducer element 2.000 × 0.110 mm^2, bandwidth 46% at −6dB, corresponding to 11-18 MHz). Image resolution is 0.110 × 0.110 mm^2. This probe has an acoustic lens with an elevation focal distance of 8 mm and an elevation focal width of 400 μm, corresponding to the thickness of the imaging plane. The active part is embedded in 18.5 mm diameter and 25 mm length molded resin. A 150cm cable length and 12 g probe weight ensure a good freedom and comfort to move for the animal. Compared to previous work [Macé et al 2011, Osmanski et al 2014], the probe was miniaturized (Supplementary Fig. 1). Dimensions (in cm) were reduced from 15 (height), 6 (width), 2.5 (thick) to 2.5 × 1.85 × 1.85. The weight (in g) was reduced from 250 to 12. The cable was made more flexible by reducing its diameter from 11.5 to 6.9 mm. All these improvements did not affect sensitivity of the transducer array and were required to perform such experiments on moving animals.

Penetration of the ultrasound waves across 15mm of rat brain allows to image rat brain at all depth (as shown in Fig. 1a, bottom image). More generally depth of penetration decreases with higher frequencies (smaller wavelength), while resolution simultaneously increases. Thus there is a tradeoff between resolution and depth of penetration, and 15 MHz is optimal for rat brain.

Although we designed the probe, it was manufactured by specialist company Vermon. Interested labs are welcome to contact us to share our customized probe design considerations.

Probe holder

The holder is made of two parts machined in Plexiglas for light weight and stiffness. First, a base plate with U-shaped side grooves, allowing translation of the mobile part, is attached to the head of the animal with three screws. Second, the mobile part presenting two sliding side edges is fitted into the base part. The probe is attached through a central opening in the mobile part. A linear servo motor (Robotshop.com, VS-19) is fixed to the mobile part and anchored on the base plate. It is controlled by custom made electronics connected to the ultrasound scanner through USB port. Holder weight is 18 g, and overall size 41 mm width, 34 mm length, 16 mm height. Digital information to reproduce the parts is provided as Supplementary file 1.

The motor of the probe holder is controlled in steps of 125 μm. Motor accuracy is better than one step. The time to travel the range of 15 mm is about 2 s. There is no need for faster motion of the motor. Rather, when hemodynamics of distinct anatomical structures have to be compared, a better strategy is to rotate the probe to image a plane encompassing those structures. Ultimately, for more complex simultaneous 3D imaging, multiple further miniaturized linear probes will be combined. The current experimental limit for imaging lies not in drifts or instability of the electro-mechanical system, but rather in the eventual leak in the prosthetic skull, generating gas bubbles that degrade imaging. This happens several weeks and up to 2 months after surgery.

Ultrasound imaging

Vascular images are obtained via the Ultrafast Compound Doppler Imaging technique [Bercoff 2009, Macé 2011]. The probe is driven by a fully programmable GPU-based ultrafast ultrasound scanner (Aixplorer, Supersonic Imagine, Aix-en-Provence, France) relying on 24 Gb RAM memory. In “burst mode” we used an acquisition sequence of 6000 frames at a rate of 500 Hz for a total acquisition time of 12 s. Manual trigger was given when the animal finished drinking water, and turned around in position for the next run. In the “continuous mode”, we acquired 200 ultrasound images at 1 kHz frame rate for 200 ms, repeating every 3 s. In both “burst mode” and “continuous mode” each frame is a Compound Plane Wave frame, that is, a coherent summation of beamformed complex in phase/quadrature images obtained from the insonification of the medium with a set of successive plane waves with specific tilting angles [Bercoff 2011]. This compound plane wave imaging technique enables to recreate a posteriori a good quality of focalization in the whole field of view with very few ultrasound emissions. Given the tradeoff between frame

rate, resolution and imaging speed, a Plane Wave Compounding using five 5°-apart angles of insonification (from −10° to +10°) has been chosen. As a result, the pulse repetition frequency (PRF) of plane wave transmissions was equal to 8 kHz. In order to discriminate blood signals from tissue clutter, the Ultrafast Compound Doppler frame stack is high pass filtered using a 4th order Butterworth filter (cut-off frequency 50 Hz) along the temporal dimension, giving a high frequency in phase/quadrature frame stack whose energy in each pixel is then computed to build the ultrafast Power Doppler fUltrasound image. Some frames are discarded before being incorporated in a recording when they show artifact echoes, which are caused by the animal bumping the probe against a hard surface such as cage or maze wall.

The signal measured by fUltrasound and its sensitivity are presented in earlier theoretical and experimental work [Macé et al 2013]. Briefly, fUS measures moving echogenic particles, that is red blood cells, and thus corresponds to cerebral blood volume (CBV). Importantly, this proportionality is valid only if backscattering properties do no vary versus time. This assumption is valid while red blood cells backscattering properties such as hematocrit and shear rate remain time-invariant, which is most likely.

Ultrasound sequences

Technical specifications of the scanner used here include 16x, 6 Gb/s PCI express bus, 12 core 3 GHz Xeon processor, NVidia Quadro K5000 GPU with a bus at 173 Gb/s, providing 2.1 Teraflops. One current limitation of fUltrasound is due to the transfer and processing time of the large amount of data required to form (“beamform”) fUS images. Yet, this limitation does not stem from physical principles, but rather from contingent hardware. Although increasing computing power and optimized software provide perspective for continuous monitoring at high speed (200ms per image), we show here that the current technology allows “continuous” recording with a temporal resolution close to the time constant of neurovascular coupling (1-2 s), and further allows “burst” capture for quick behavioral events such as running a maze (Supplementary Fig. 7). The limitation for the “continuous” mode is the processing speed to transform a series of plane wave acquisitions into compound images and then generate a fUltrasound image. The limitation for the “burst” mode is the memory available to buffer plane wave images to later generate a movie of fUltrasound images. We provide matlab code archive for these sequences as Supplementary file 2.

Ultrasound stability and reproducibility

Stability during a recording session and across sessions is estimated from our recordings. Variation during a recording is exemplified on Figure 2b, with narrow standard deviation around average traces. This indicates good stability during a recording session. Reproducibility across recordings is quantified on Figure 2c, g which summarize measures across all animals. It shows a good reproducibility.

We cannot completely exclude a contribution of a locomotion effect, for instance due to higher heart rate during running. However, the maze task is not limited to running, as it clearly involves navigation processing. Animals show a learning curve when they train for

the task. Furthermore, a locomotion effect would likely be uniform across the brain, whereas we find both increases and decreases in blood perfusion. Thus, such a potential effect is not strong enough to mask differential changes and dynamics across areas. Our animals did not engage in intensive motor activity, at least not above the requisite for most cognitive and pathology experiments. GAERS rats seizures correspond to freezing behavior, and yet again they exhibit increases and decreases of similar amplitude compared to moving animals. This further supports that the technique can sense changes in perfusion unrelated to a locomotion effect.

EEG acquisition

Intracranial electrode signals are fed through a high input impedance, DC-cut at 1 Hz, gain of 1000, 16 channel amplifier and digitized at 20 kHz (Xcell, Dipsi, Cancale, France), together with a synchronization signal from the ultrasound scanner. Custom made software based on Labview (National Instruments, Austin, TX, USA) simultaneously acquires video from a camera pointed at the recording stage.

Contrary to fMRI, which generates strong magnetic field, there is no such cause for artifact with ultrasound. A regular amplifier is used, and no additional electronic circuit for artifact suppression is necessary. A large bandwidth amplifier was used, which can record both local field potentials (LFP, 0.1-200 Hz) and multiunit activity (MUA, 200-2 kHz), although we did not need this later feature in the work presented here. The spatial resolution of LFPs remains controversial depending on recording location and parameters, with estimates ranging from 250 μm to several mm radius. MUA radius of detection is around 70-200 μm.

Analysis software

Data is collected from ultrasound and video-EEG devices for offline processing. We implemented the analysis software with Labview, with sample data and code archive provided as a Supplementary file 3. We suggest interested labs to contact us for further enquiry in the algorithm.

Analysis algorithms

Animal position is detected by applying a threshold on the image pixel intensity that distinguish the bright animal on dark background. Cumulative distance and maximum crossing speed are computed using the trajectory smoothed with a time constant of 0.5s.

Ultrasound images are normalized according to the average value over all the non-running or non-seizing time, thus giving the relative change in vascular echo in percent of baseline. Paxinos atlas is superimposed using the cortex as the main landmark. Statistical significance on images used Bonferroni correction to account for the multiple testing over the large number of pixels.

EEG is filtered pass-band 6-9Hz for hippocampal theta. Power of theta is computed as the square of the EEG signal integrated over a sliding window of characteristic width 0.5s.

Epileptic seizures are detected when EEG electrodes presents at least 3s of spikewave at a rate above 5Hz, while a spikewave interval of 3s discriminates consecutive seizures.

Seizures are defined on the EEG alone and are always bilateral. Since we use bipolar recording that ensure locality of the EEG close to each recording bipolar electrode, and as it is well accepted, the electrographic signs of seizures are bilateral. In Figure 2d we show in color code Pearson's correlation coefficient between EEG defined seizures and pixel intensity. This is how we determine the vascular correlate of seizures, which often appears asymmetric, contrary to the EEG.

Computation of Pearson's R correlation coefficient between EEG and mfUS pixel intensity is based on theta power curve for the maze experiment. For the epilepsy experiment pixel intensity is correlated to seizure status function (1 inside seizure, 0 outside). Statistical test is performed on Pearson's R coefficient using Student's t-distribution.

All statistics are given as mean+/−standard deviation.

Supplementary Material

Refer to Web version on PubMed Central for supplementary material.

Acknowledgments

The authors gratefully acknowledge E. Yeramian and A. Bonnot for critical discussions and help with the manuscript.

The research leading to these results has received funding from the European Research Council under the European Union's Seventh Framework Programme (FP7/2007-2013) / ERC grant agreement n° 339244-FUSIMAGINE. This work was also partly supported by the Agence Nationale de la Recherche under the program “Future Investments” with the reference Laboratory of Excellence ANR-10-LABX-24 LABEX WIFI within the French Program “Investments for the Future” under reference ANR-10-IDEX-0001-02 PSL and the program “Investissements d'avenir” ANR-10-IAIHU-06.

Bibliography

Bercoff J, Montaldo G, Loupas T, Savery D, Meziere F, Fink M, Tanter M. Ultrafast Compound Doppler Imaging: Providing Full Blood Flow Characterization. IEEE Trans. Ultrason. Ferroelectr. Freq. Control. 2011; 58:134–147. [PubMed: 21244981]

Brincat SL, Miller EK. Frequency-specific hippocampal-prefrontal interactions during associative learning. Nat Neurosci. 2015

Buzsáki G, Moser EI. Memory, navigation and theta rhythm in the hippocampalentorhinal system. Nat Neurosci. 2013; 16(2):130–8. [PubMed: 23354386]

David O, Guillemain I, Saillet S, Reyt S, Deransart C, Segebarth C, Depaulis A. Identifying neural drivers with functional MRI: an electrophysiological validation. PLoS Biol. 2008; 6(12):2683–97. [PubMed: 19108604]

Jacobs J, Levan P, Moeller F, Boor R, Stephani U, Gotman J, Siniatchkin M. Hemodynamic changes preceding the interictal EEG spike in patients with focal epilepsy investigated using simultaneous EEG-fMRI. Neuroimage. 2009; 45(4):1220–31. [PubMed: 19349236]

Kerr JN, Nimmerjahn A. Functional imaging in freely moving animals. Curr Opin Neurobiol. 2012; 22(1):45–53. [PubMed: 22237048]

Koehler RC, Roman RJ, Harder DR. Astrocytes and the regulation of cerebral blood flow. Trends Neurosci. Mar; 2009 32(3):160–9. [PubMed: 19162338]

LaMendola NP1, Bever TG. Peripheral and cerebral asymmetries in the rat. Science. 1997; 278(5337): 483–6. [PubMed: 9334310]

Logothetis NK. What we can do and what we cannot do with fMRI. Nature. 2008; 453(7197):869–78. [PubMed: 18548064]

Logothetis NK, Eschenko O, Murayama Y, Augath M, Steudel T, Evrard HC, Besserve M, Oeltermann A. Hippocampal-cortical interaction during periods of subcortical silence. Nature. 2012; 491(7425):547–53. [PubMed: 23172213]

Macé E, Montaldo G, Cohen I, Baulac M, Fink M, Tanter M. Functional ultrasound imaging of the brain. Nat. Methods. Jul.2011 8(no. 8):662–664. [PubMed: 21725300]

Mace E, Montaldo G, Osmanski B, Cohen I, Fink M, Tanter M. Functional ultrasound imaging of the brain: theory and basic principles. IEEE Trans. Ultrason. Ferroelectr. Freq. Control. 2013; 60(no. 3):492–506. [PubMed: 23475916]

Mishra AM, Ellens DJ, Schridde U, Motelow JE, Purcaro MJ, DeSalvo MN, Enev M, Sanganahalli BG, Hyder F, Blumenfeld H. Where fMRI and electrophysiology agree to disagree: corticothalamic and striatal activity patterns in the WAG/Rij rat. J Neurosci. 2011; 31(42):15053–64. [PubMed: 22016539]

O'Neill PK, Gordon JA, Sigurdsson T. Theta oscillations in the medial prefrontal cortex are modulated by spatial working memory and synchronize with the hippocampus through its ventral subregion. J Neurosci. 2013; 33(35):14211–24. [PubMed: 23986255]

Osmanski BF, Pezet S, Ricobaraza A, Lenkei Z, Tanter M. Functional ultrasound imaging of intrinsic connectivity in the living rat brain with high spatiotemporal resolution. Nat Commun. 2014; 5:5023. [PubMed: 25277668]

Packer AM, Russell LE, Dalgleish HW, Häusser M. Simultaneous all-optical manipulation and recording of neural circuit activity with cellular resolution in vivo. Nat Methods. 2015; 12(2):140–6. [PubMed: 25532138]

Paxinos, G.; Watson, C. The rat brain in stereotaxic coordinates. 6th Edition. Academic Press; 2007.

Roche-Labarbe N, Zaaimi B, Mahmoudzadeh M, Osharina V, Wallois A, Nehlig A, Grebe R, Wallois F. NIRS-measured oxy- and deoxyhemoglobin changes associated with EEG spike-and-wave discharges in a genetic model of absence epilepsy: the GAERS. Epilepsia. 2010; 51(8):1374–84. [PubMed: 20412285]

Sada N, Lee S, Katsu T, Otsuki T, Inoue T. Epilepsy treatment. Targeting LDH enzymes with a stiripentol analog to treat epilepsy. Science. 2015; 347(6228):1362–7. [PubMed: 25792327]

Zheng TW1, O'Brien TJ, Morris MJ, Reid CA, Jovanovska V, O'Brien P, van Raay L, Gandrathi AK, Pinault D. Rhythmic neuronal activity in S2 somatosensory and insular cortices contribute to the initiation of absence-related spike-and-wave discharges. Epilepsia. 2012; 53(11):1948–58. [PubMed: 23083325]

Europe PMC Funders Author Manuscripts

Europe PMC Funders Author Manuscripts

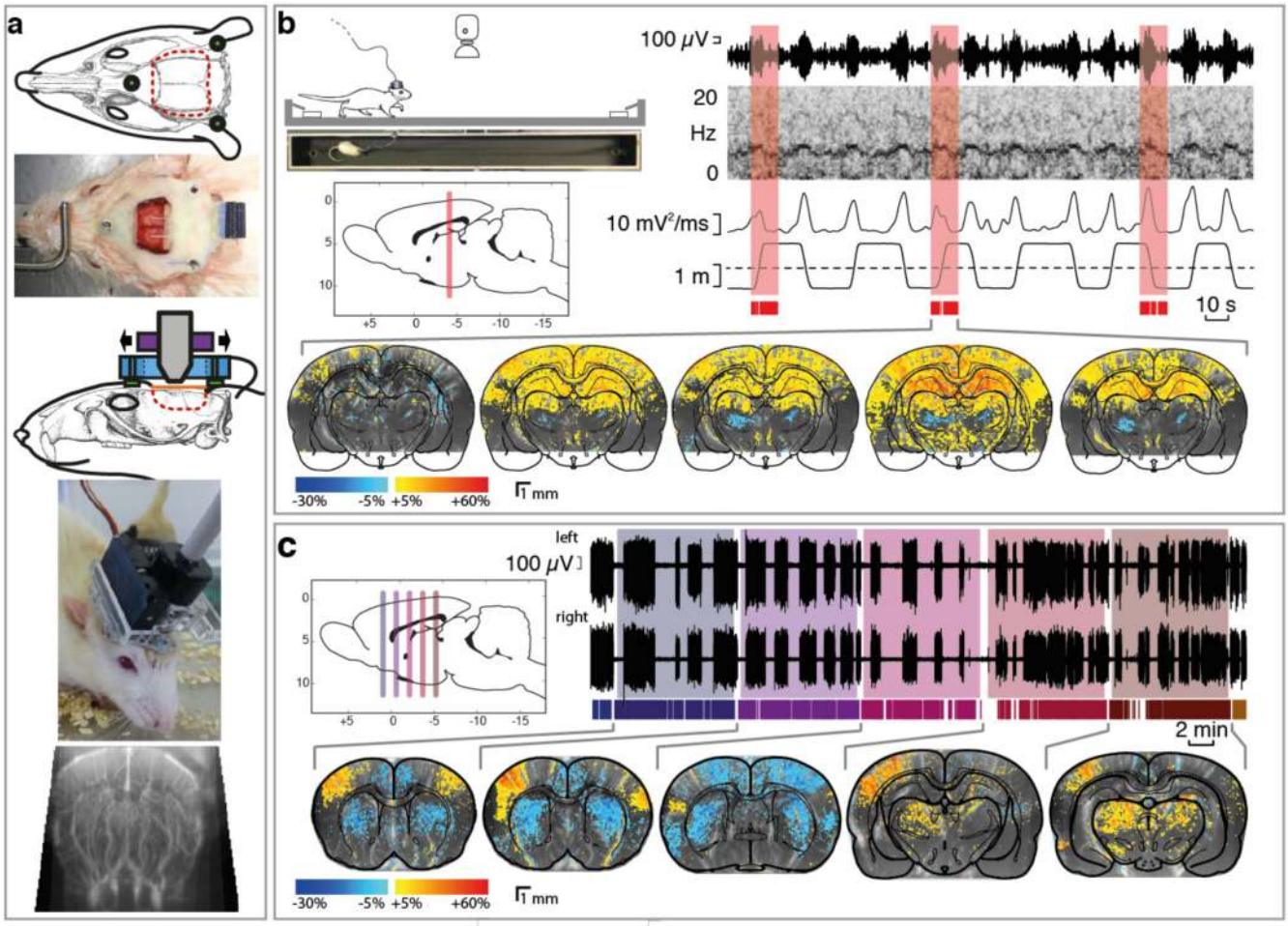

Figure 1.

Awake/mobile EEG-fUltrasound procedure and acquisition protocols

a, Surgical procedure and probe setup. Schematic representation of window boundary (red dotted line), prosthetic skull (orange), attachment nuts (green), probe holder (blue), motor (purple) and probe (grey); Surgery outcome with added hippocampal stereotaxic electrode and EEG connector; Animal equipped with motorized translation stage; raw mfUS view through the prosthesis.

b, "burst mode" acquisition for maze experiments. Schematic of the maze, water reward sites and overhead camera. Inset, atlas side view with the coronal imaging plane shown as red bar. Right: EEG-behavior recording chart from top to bottom, hippocampal local field potential (LFP), Short Term Fourier Transform spectrum, and power in the theta band. The lower trace shows position along the maze, bottom red bars indicate timing of fUltrasound images. Hippocampal theta exhibits modulation during the task. Its peak corresponds to top speed and mid-maze crossing (dotted line), used as a time reference. The red boxes represent the 12 s frames of fUltrasound acquisition. Coronal ultrasound images acquired at high speed are averaged (n=25 runs) for an example of 5 consecutive times around the reference. Color coded overlay on vascular background shows pixel intensity change relative to baseline rest. Ventral areas were not acquired to increase burst duration.

c, “continuous mode” acquisition for seizure recording. Spontaneous generalized absence seizures are recorded from bilateral EEG. fUltrasound image trigger mark is shown below the EEG. Coronal planes indicated in the inset are acquired successively for 10 min each. Each color corresponds to a coronal plane. Color coded overlay on vascular background shows pixel intensity change relative to baseline outside seizure.

b, c, Changes in pixel intensity relative to baseline is shown where $p<10^{-2}$ (Student test with Bonferroni correction). Overlay from Paxinos atlas [Paxinos 2007]

Europe PMC Funders Author Manuscripts

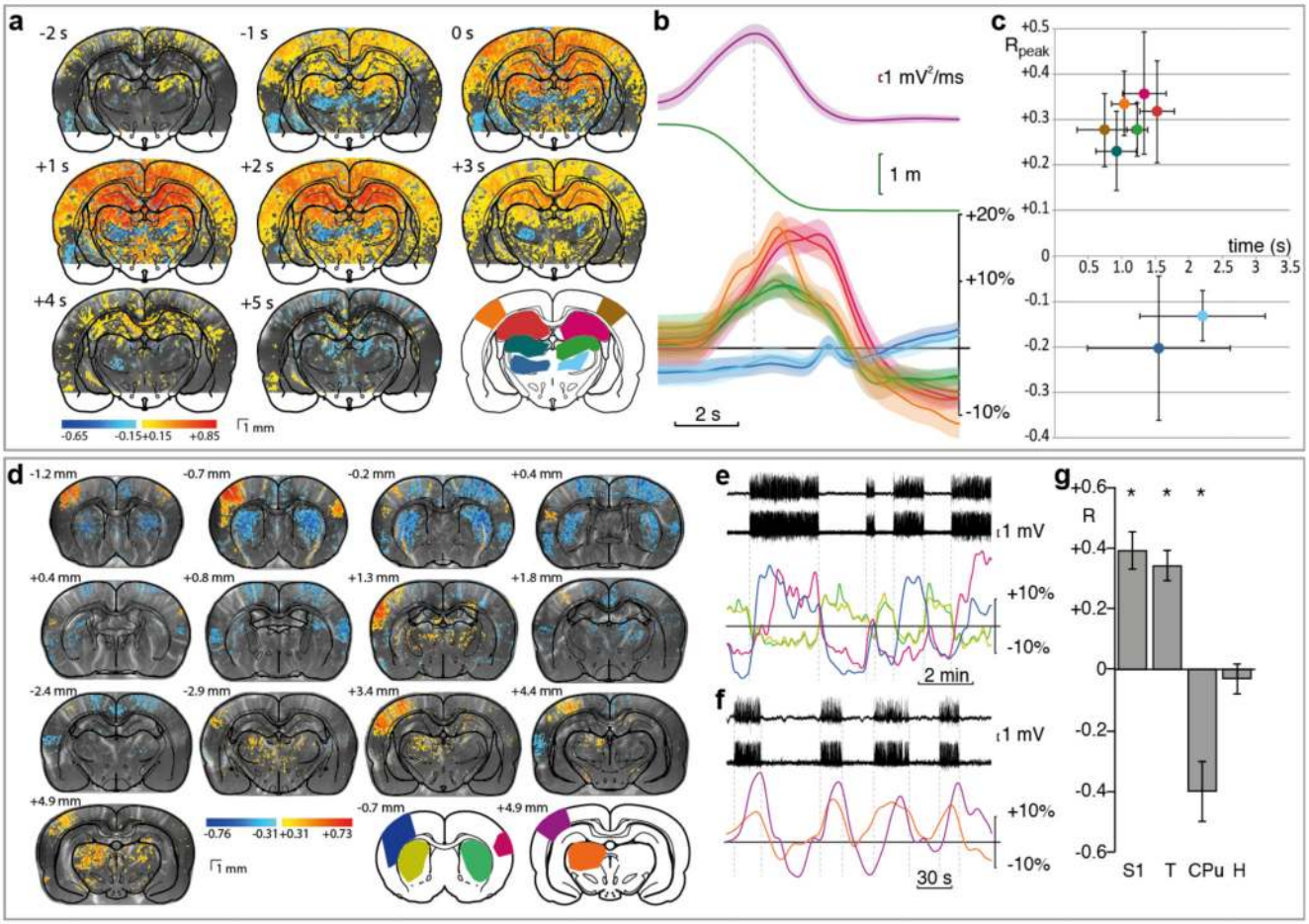

Figure 2.

Comparison of EEG and hemodynamic signatures of natural events

a-c, Maze experiment cross-correlation (a) between LFP theta band power and ultrasound signal for each pixel at varying time lag (−2 to +5 s) over n=20 midline crossings acquired in one hour. Widespread hyper-perfusion occurred between −1 and +3s, together with hypo-perfusion in ventral thalamus. Region variation of hemodynamic signal, relative to rest, is obtained by spatial averaging of pixels indicated on atlas layout (mean+/−sd envelop). Mean theta power (purple) and trajectory (green). The vertical dotted line shows the reference midline-crossing time (b). Value and delay of peak Pearson's R (c) show close responses between left and right dorsal thalamus, hippocampus, and primary sensory cortex (n=6 animals).

d-g, Epilepsy experiment cross-correlogram between mfUS image and seizure, at zero time lag, for successive coronal planes (d). The sensory cortex showed several hyper-perfusion patches on one hemisphere and none on the other. Caudal thalamus was also significantly hyper-perfused. Hypo-perfusion was found in the CPu and some cortical areas. Averaging areas color-marked on atlas layouts showed bilateral fluctuations in the CPu (e). On the contrary, the cortex showed transient bilateral or unilateral co-activation, even though seizures were always bilateral on the EEG. Synchronous oscillations in the seizing cortex and thalamus were found in caudal planes (f). Average over significant areas (g) consistently

Europe PMC Funders Author Manuscripts

showed hyperperfusion in sensory cortex and thalamus versus hypoperfusion in CPu, and stable hippocampus perfusion (n=6 animals).

a, d Cross-correlation Pearson's R coefficient is color coded according to bottom color scales. Significant pixels are shown for $p<10^{-2}$ with Bonferroni correction.

Europe PMC Funders Author Manuscripts